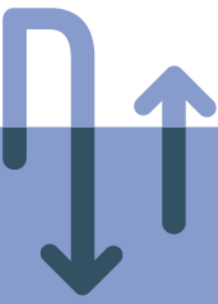


scan 



# Estimating geothermal power of ultra-deep Dinantian carbonates in the Dutch subsurface

Report by SCAN  
September 2019

*This page intentionally left blank*

# Estimating geothermal power of ultra-deep Dinantian carbonates in the Dutch subsurface

Written by:  
Pieter Bruijnen<sup>1</sup>

September 2019

1-Energie Beheer Nederland (EBN), Daalsesingel 1, 3511 SV Utrecht, the Netherlands

*Dit rapport is een product van het SCAN-programma en wordt mogelijk  
gemaakt door het Ministerie van Economische Zaken en Klimaat*

*This page intentionally left blank*

## Contents

1. Executive summary / Samenvatting.....	6
1.1. Executive summary.....	6
1.2. Samenvatting.....	6
2. Introduction.....	8
3. Single well performance versus doublet performance .....	9
4. Three-phase approach for geothermal power calculation .....	9
5. Normalised Capacity Index.....	11
6. Step 1: reservoir modelling .....	12
6.1. Mathematical representation of naturally fractured reservoirs .....	12
6.2. Numerical approach.....	12
6.3. Analytical approach .....	13
6.4. Fracture porosity and fracture permeability.....	14
6.5. Karstification.....	14
6.6. Benchmarking .....	15
6.7. Input data and assumptions .....	15
6.8. Results.....	17
7. Step 2: wellbore modelling .....	19
7.1. Doublet modelling .....	19
7.2. Input data and assumptions .....	22
7.3. Results.....	23
8. Step 3: Compensation for overpressure .....	26
8.1. Input data and assumptions .....	26
8.2. Results.....	26
9. Workflow summary and example .....	27
9.1. Example .....	27
10. Conclusions.....	28
11. References.....	29
12. Appendix: Eclipse deck .....	30

# 1. Executive summary / Samenvatting

## 1.1. Executive summary

The aims of this study are:

- To explore the range in geothermal potential from Ultra-Deep Geothermal (UDG) doublets in Dinantian carbonates in the Dutch subsurface. Results from other studies on Dinantian carbonates will be used as input.
- To provide a first-pass screening workflow for the estimation of UDG powers.
- To highlight unknowns and sensitivities in the geological input parameters, and hence in well design, resulting in a large range of uncertainty in estimated geothermal powers.

The most important geological input parameters that are needed in order to quantify the geothermal power of naturally fractured carbonates include fracture aperture, fracture spacing, matrix porosity, matrix permeability, reservoir depth and reservoir pressure. Geological information regarding the Dinantian carbonates in the Dutch subsurface is relatively scarce and crucial geological data carry a rather large degree of uncertainty. The wide range in possible values of these parameters makes a detailed well design not possible at this exploratory phase. Well design including well length and well diameter thus carries uncertainty as well. Consequently, the models to calculate the geothermal power carry the same degree of uncertainty, resulting in uncertainties in estimated doublet's performances.

For this reason, a workflow is provided in this report that allows the reader to determine the geothermal power from UDG doublets, based on assumptions yet to be made. This workflow consists of a series of graphs, which can be used to determine the geothermal power of UDG doublets. It is recommended to make informed decisions regarding the input data, and to subsequently use this set of graphs to calculate the first-pass geothermal powers.

One must bear in mind that the correctness or accuracy of the input data fully dictates the correctness of the results. It is also important to realise that the provided set of graphs is based on the mathematical performance of a pair of wells, not taking reservoir heterogeneity, connectivity and cold water breakthrough into account.

Within the legal framework, a technical upper limit prevents unconstrained production and injection. In case the encountered reservoir properties are too poor, the resulting geothermal power may not be sufficient for a good business case. The technical and economic limits result in a certain bandwidth of geothermal power. This bandwidth must be explored further in order to assess the economic viability of UDG doublets.

## 1.2. Samenvatting

De doelen van deze studie zijn als volgt:

- Het bepalen van de spreiding in geothermisch vermogen van ultradiepe geothermische (UDG) doubletten in het Nederlandse Dinantien.
- Het bieden van een first-pass screening workflow om het UDG vermogen te bepalen.
- Het aangeven van onbekenden en gevoeligheden binnen de geologie en daarmee het gepaard gaande put ontwerp, wat resulteert in een spreiding in geothermische vermogens.

De belangrijkste geologische variabelen die noodzakelijk zijn om het geothermisch vermogen van natuurlijk verbreukt carbonaat gesteenten te kwantificeren, zijn breukvlak opening, breukvlak verspreiding, matrix porositeit, matrix permeabiliteit, reservoir diepte en reservoir

druk. Geologische informatie betreffende carbonaat gesteenten uit het Dinantien in de Nederlandse ondergrond is relatief zeldzaam en cruciale geologische data heeft een grote mate van onzekerheid. Door de grote spreiding in mogelijke waarden van deze variabelen is een gedetailleerd put ontwerp gedurende deze exploratie fase niet mogelijk. Daardoor zijn put lengte en put diameter ook onzeker. Modellen om het geothermisch vermogen te berekenen dragen als gevolg hiervan diezelfde onzekerheid met zich mee, wat resulteert in onzekerheden in de uitkomsten.

Om deze reden wordt in dit document een workflow gegeven, waarmee de lezer het geothermisch vermogen kan bepalen, op basis van aannames die nog gemaakt moeten worden. Deze workflow bestaat uit een reeks grafieken die gebruikt kunnen worden om het geothermisch vermogen van UDG doubletten te bepalen. Het is van belang om weloverwogen beslissingen te nemen over de data die nodig zijn voor deze workflow, zodat met behulp van deze grafieken een eerste orde berekening van het geothermisch vermogen uitgevoerd kan worden.

Het is belangrijk om te beseffen dat de juistheid of de nauwkeurigheid van de input data de juistheid van de resultaten bepaalt. Het is ook belangrijk om te beseffen dat de reeks grafieken in dit document gebaseerd zijn op de wiskundige resultaten van slechts twee putten, waarbij reservoir heterogeniteit, connectiviteit en kou doorbraak niet zijn.

Binnen het juridisch kader is er een technische limiet die de operator ervan weerhoudt onbeperkt te produceren en te injecteren. In het geval dat de aangetroffen reservoir eigenschappen niet goed genoeg blijken te zijn, zal het geothermisch vermogen ontoereikend zijn voor een goede business case. Deze technische en economische limieten resulteren in een bepaalde bandbreedte in geothermisch vermogen. Deze bandbreedte moet verder onderzocht worden om UDG doubletten economische haalbaar te maken.

## 2. Introduction

Geothermal energy systems have been considered as a potential alternative for the fossil energy use. Currently, geothermal systems are already in use in the Netherlands. However, the application of geothermal energy in existing projects is not adequate for the provision of high-temperature heat for, as an example, the process industry. It is anticipated that ultra-deep geothermal (UDG) energy could potentially make a substantial contribution to the transition towards a sustainable energy supply. To reach sufficiently high temperatures ( $>130^{\circ}\text{C}$ ) in the Netherlands, geothermal reservoirs at depths of over 4 km are required. The Dutch subsurface at these depths has not been explored extensively until now and is therefore relatively unknown. Based on the limited amount of subsurface data, the Lower Carboniferous (Dinantian) carbonates were identified by Boxem et al. (2016) as the most promising target matching the initial requirements for UDG.

The study reported in this document is a result of SCAN, a government funded program to scope out the potential of geothermal energy, including the Dinantian carbonates. This program includes a range of subsurface studies of the Dinantian carbonates. The results of the SCAN studies will be released and become available via [www.nlog.nl](http://www.nlog.nl) and <https://scanaardwarmte.nl/>.

The subsurface study described in this document builds on the other SCAN studies, and involves the determination of the range in possible geothermal powers that can be achieved by production from ultra-deep naturally fractured Dinantian carbonates. The aim of this report is not only to deliver a variety of possible outcomes, in the form of a set of graphs, but also to create awareness that exploring the relatively unknown Lower Carboniferous comes with uncertainty regarding the geothermal potential of this play. The large number of unknowns has led to the unavoidable decision that a workflow is provided to calculate the geothermal power, rather than directly providing the geothermal flow potential of a doublet. This workflow is based on a range of geological parameters and various well design options and can be used as a screening device for first pass assessment of the geothermal potential for UDG doublets in the Dinantian.

### 3. Single well performance versus doublet performance

The ultra-deep Dutch subsurface has not been explored extensively yet and is therefore associated with high levels of uncertainty regarding the geological properties and reservoir architecture. Only 26 wells penetrate the Dinantian of which 11 wells have a comprehensive set of logs, the geological and petrophysical evaluation of which has been described by e.g. Carlson (2019), Mozafari et al. (2019) and Van Leverink and Geel (2019).

Naturally fractured carbonates are geologically complex and production data from ultra-deep Dinantian reservoirs are absent. Furthermore, the lack of dense well spacing, in combination with limited depth control due to poor seismic data, poses several problems for reliable prediction of geothermal powers from UDG doublets. Firstly, the geological properties that determine the performance of a single well are largely unknown, and it is questionable to what extent the existing wells are representative for wells yet to be drilled in new locations. Consequently, the prediction of the productivity or injectivity of individual wells carries uncertainty. Secondly, the internal facies distribution and diagenesis within a single carbonate reservoir is often much more complex and heterogenous than for example sandstone reservoirs. In addition to the sedimentary and diagenetic heterogeneity (Mozafari et al., 2019), the fracture geometry within the Dinantian is also largely unknown and uncertain (Van Leverink and Geel, 2019). This makes the intra-well connectivity uncertain too. Due to the lack of production data from ultra-deep carbonates, it is not possible to confirm the correctness of complex and detailed reservoir models. For these reasons, the decision was made not to pursue the construction of detailed reservoir models that can be used to predict the connectivity and breakthrough time of carbonates. Single (mathematical) well models were used instead, which do not take the connectivity between the injector and the producer into account; it is not until the two wells are drilled that the connectivity between them can be determined. Although there is no reason to assume that the wells are not connected, theoretically doublets might not behave conform the predictions outlined in this document in case reservoir connectivity is not established. Another consequence of using single well models instead of geologically complex 3-dimensional reservoir models is that the cold water breakthrough time cannot be modelled; the performance of the doublet as highlighted in this document does not take early breakthrough into account.

Although these simplifications might not be realistic in a geological context, the lack of data leaves no alternatives. At this exploratory phase it is important to realise that well performance predictions come with a range, rather than with a discrete value, and that (dis)connectivity can impact the well's performance over the life-time of the doublet. The same applies for well stimulation or well deterioration over time. Carbonate reservoirs might be suitable candidates for well stimulation in case of unsatisfactory capacity. On the other hand, operational practices can heavily impair the injector's performance as well. These operational aspects are not considered in the calculation of the doublet's performance in this report.

### 4. Three-phase approach for geothermal power calculation

The primary goal of this study is to explore the range in geothermal power for ultra-deep Dinantian reservoirs, and to highlight sensitivities and unknowns for geological parameters, well design and subsequently geothermal power. The intrinsic dilemma for projects at such an exploratory phase is the number of parameters that require quantification in order to determine the actual potential in geothermal power. Based on the sparse data available from wells drilled into the Dutch Dinantian and from seismic data, a geological characterization of the Dinantian carbonates in the Netherlands has been done within the SCAN program, see

Mozafari et al. (2019) and Bouroullec et al. (2019). An extensive petrophysical analysis for the Dinantian carbonates and review of well reports is made by Carlson (2019). The ranges of uncertainty for geological parameters are large, thus making the ranges in geothermal powers large as well. The main unknown variables that control the geothermal power are shown in Figure 1 :

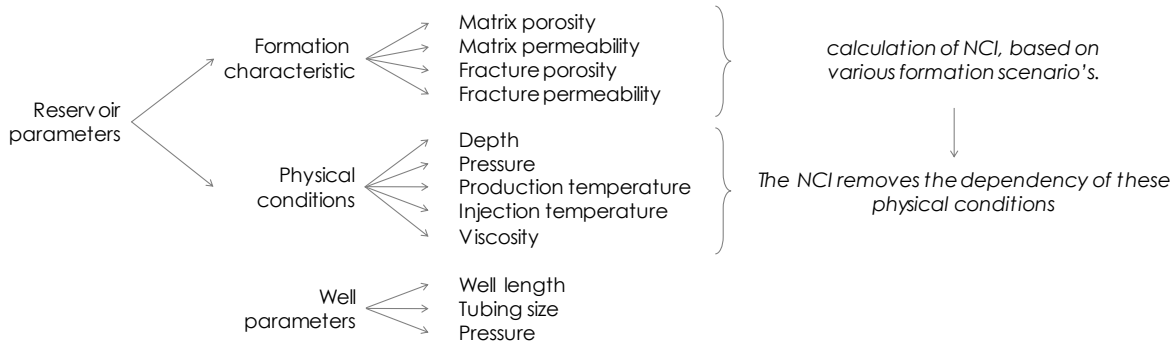


Figure 1. Unknown variables that control the geothermal power

Due to limited data availability and the lack of existing producing ultra-deep Dinantian wells, the number of unknowns cannot be reduced any further, resulting in a multi-dimensional problem with an almost infinite amount of solutions. In order to cope with this, the concept of Normalised Capacity Index (NCI) was developed to characterize reservoirs. The NCI is an intrinsic reservoir property and is a measure for the performance of formations. The concept of NCI is discussed in detail in chapter 5.

Determination of the geothermal power for Dinantian doublets was done in three steps. The first step involves reservoir characterization. Calculation of various NCIs, based on realistic assumptions for the formation characteristics, was done in Eclipse (Schlumberger, 2019) and benchmarked with Prosper (Petroleum Experts, 2019). The end product of this step is a set of graphs which allows the user to determine the NCI for every combination of formation characteristics.

Step 2 involves wellbore modelling, based on the NCI calculated in step 1, and on well characteristics like tubing/casing diameter and well depth. Wellbore modelling involves the calculation of the flowrates and accompanying pressure drops, via a set of fluid flow equations. EBN's inhouse software 'THOR' was used for this nodal analysis approach. The end product of step 2 is a set of graphs, which allows the user to determine the geothermal power of a doublet, provided that the reservoir is not overpressured.

In step 3 the effect of overpressure is accounted for, since overpressure does have a negative impact on the geothermal power. The end product of step 3 is a set of graphs, which allows the user to determine the reduction in geothermal power per bar overpressure.

All three steps combined can be used as a screening device for first pass assessment of the geothermal potential for UDG doublets in the Dinantian.

## 5. Normalised Capacity Index

The conventional Productivity Index is the ratio between the total liquid flow rate and the pressure drawdown, and the steady state approximation for a vertical well is mathematically given as (Dake, 1978):

$$Productivity\ Index = \frac{Q_w}{(\Delta P_{producer})} = \frac{2\pi kh}{\mu_{producer} \left[ \ln\left(\frac{r_e}{r_w}\right) + S \right]} \quad [1]$$

where  $Q_w$  is the water production rate,  $\Delta P_{producer}$  is the pressure difference (drawdown) between the external boundary of the reservoir and the flowing bottomhole pressure at the sandface,  $h$  is reservoir thickness,  $\mu_{producer}$  is fluid viscosity,  $r_e$  reservoir radius,  $r_w$  is wellbore radius and  $S$  is the skin factor. In the context of naturally fractured reservoirs,  $k$  is the “effective” permeability, accounted for the occurrence of natural fracs. For gas-free hydrothermal water, the productivity index is depicted as a straight line on a  $P_{wf}$  v.s.  $Q_w$  graph, see Figure 2. The PI thus is a single number reflecting the ability to produce from the reservoir, and is dictated by reservoir properties (e.g. permeability, thickness, fractures, etc) and the viscosity in the *produced* fluid. The PI is also independent of reservoir pressure: if the reservoir pressure changes, the slope of the PI-line in Figure 2 remains unchanged.

Likewise, the Injectivity Index reflects the injection performance of a well, and is dictated by the reservoir properties around the injection well (e.g. permeability, thickness, fractures, etc.) and the viscosity of the *injected* fluid, see equation below:

$$Injectivity\ Index = \frac{Q_w}{(\Delta P_{injector})} = \frac{2\pi kh}{\mu_{injector} \left[ \ln\left(\frac{r_e}{r_w}\right) + S \right]} \quad [2]$$

Since the viscosity of the (cold) injected fluid is always higher than the viscosity of the (warm) produced fluid, the injectivity index will always be lower than the productivity index (assuming equal reservoir properties), see Figure 2. This makes a comparison between the performance of the injector and producer (or amongst different doublets in different geological settings) difficult, since the viscosity effect is included in the equations or graphs. Multiplying (i.e. normalising) either the productivity index or the injectivity index with the viscosity at the prevailing temperatures, results in a single index, which is representative for both the injector and producer (assuming equal reservoir properties and well diameter). This index is called the Normalised Capacity Index (NCI), see Figure 2. Mathematically:

$$NCI = Productivity\ Index \cdot \mu_{producer} = Injectivity\ Index \cdot \mu_{injector} \quad [3]$$

One of the main advantages of the concept of Normalised Capacity Index is that the NCI is not only independent of pressure (just like the productivity index and the injectivity index), but is also independent of the depth, temperature, viscosity and well type (producer v.s. injector). By removing the dependency on pressure, depth, temperature and viscosity, the number of variables required to quantify the performance of (naturally fractured) reservoirs is reduced drastically. This reduction facilitates and simplifies the forecasts of the doublet performances. The NCI also allows to make an easy and fair comparison of the reservoirs between the injector and the producer, and between doublets from other formations with different characteristics.

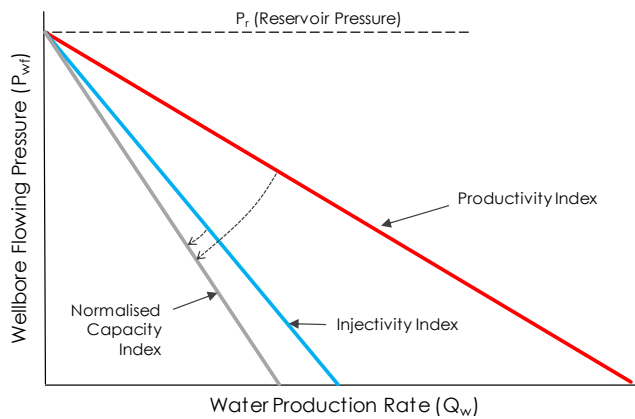


Figure 2. Relation between Productivity Index (red), Injectivity Index (blue), and Normalised Capacity Index (grey)

## 6. Step 1: reservoir modelling

### 6.1. Mathematical representation of naturally fractured reservoirs

Naturally fractured reservoirs in general consist of two interconnected systems: the rock matrix and highly permeable natural fractures. Mathematically, naturally fractured reservoirs can be modelled either numerically or (semi)-analytically.

### 6.2. Numerical approach

Eclipse 100 (Schlumberger, 2019) has been used to numerically model the reservoir's productivity and injectivity. To model naturally fractured reservoirs in Eclipse, two simulation cells are associated with each block in the geometric grid, representing the matrix and fracture volumes of the cell. Their properties are defined independently, and a matrix-fracture coupling transmissibility ("sigma") is constructed to simulate the flow between the two systems. A schematic visualisation of this mathematical representation of naturally fractured reservoirs is shown in Figure 3. In this "sugar cube" model the sugar cubes represent the matrix, with its specific reservoir porosity and reservoir permeability, while the space in between the sugar cubes represent the fractures, of which the relevant characteristics are the spacing (or density) and aperture.

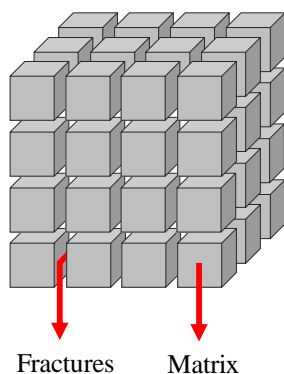


Figure 3. Schematic visualisation of the mathematical representation of naturally fractured reservoirs.

The interaction between the fractures and the matrix largely determines the flow behaviour of the rocks, both in reality and in software. If the matrix blocks are linked only through the

fracture system, this is considered to be “dual porosity, single permeability”, or “double porosity” for short. In such a system the fluids only flow from the fractures into the wellbore. If, however, flow between neighbouring matrix blocks takes place, a “dual porosity, dual permeability”, or a “double permeability” system is more appropriate. In this system the fluids flow from the fractures and the matrix into the well. A schematic representation of the double porosity and double permeability models is shown in Figure 4.

The matrix-fracture coupling transmissibility is calculated in Excel using Kazemi’s approach (1976) and used directly as input for Eclipse. Kazemi (1976) proposed the following formula to determine the matrix-fracture coupling transmissibility ( $\sigma$ ):

$$\sigma = 4 \left( \frac{1}{l_x^2} + \frac{1}{l_y^2} + \frac{1}{l_z^2} \right) \quad [4]$$

where  $l_x$ ,  $l_y$  and  $l_z$  are typical X, Y and Z dimensions (m) of the blocks of material making up the matrix volume. Other fracture-related input data required for Eclipse simulations include fracture porosity and fracture permeability, which are described below.

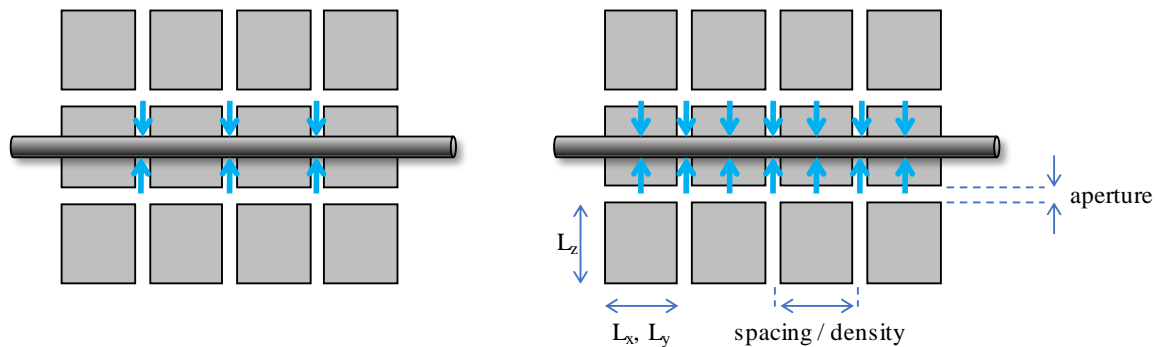


Figure 4. Schematic representation of a double porosity system (left) and a double permeability system (right).

### 6.3. Analytical approach

Prosper (Petroleum Experts, 2019) has been used to model the reservoir’s productivity and injectivity (semi)-analytically. Prosper follows the method originally developed by Warren and Root (1963). In this method, semi-steady state flow between fractures and matrix is assumed, and only the fractures contribute to well production. As such, this method follows a double porosity approach as well, see Figure 4.

In addition to fracture permeability and fracture porosity, other fracture related input includes the storativity ratio and the interporosity flow coefficient. The storativity ratio is a measure of the relative fracture storage capacity in the reservoir, and is defined as (Petroleum Experts, 2019):

$$\omega = \frac{\varphi_f c_f}{\varphi_f c_f + \varphi_m c_m} \quad [5]$$

where  $\omega$  is the storativity ratio,  $\varphi$  is the ratio of the pore volume of one medium to the total volume of that medium, and  $c$  is the compressibility. Subscripts  $f$  and  $m$  refer to fracture and matrix respectively.

The interporosity coefficient is a measure of how easily fluid flows from the matrix to the fractures, and is defined as:

$$\lambda = \alpha r_w^2 \frac{k_m}{k_f} \quad [6]$$

where  $\lambda$  is the interporosity flow coefficient,  $\alpha$  is a geometric shape factor,  $r_w$  is the wellbore radius,  $k_m$  is the permeability of the matrix and  $k_f$  is the permeability of the fracture system. The geometric factor  $\alpha$  accounts for the shape of the matrix blocks and is defined as:

$$\alpha = \frac{4n(n+2)}{\sigma} \quad [7]$$

where  $n$  is the number of fracture planes, and  $\sigma$  is the matrix-fracture coupling transmissibility as described above. This set of equations allows to solve the Warren & Root solution in a semi-analytical way.

#### 6.4. Fracture porosity and fracture permeability.

For both the numerical and the semi-analytical solutions the fracture porosity and the fracture permeability is required. Calculation of these properties is based on the model described by Reiss (1980), and the assumption is made that the length of the three dimensions (X, Y and Z) of typical matrix blocks are equal. The fracture porosity is calculated using the following equation:

$$\phi_f = \frac{(3b)}{a} \quad [8]$$

where  $\phi_f$  is the fracture porosity,  $a$  is fracture spacing (cm), and  $b$  is the fracture aperture ( $\mu\text{m}$ ). The fracture permeability is calculated using the following equation:

$$k_f = 0.62a^2\phi_f^3 \quad [9]$$

where  $k_f$  is fracture permeability (mD),  $a$  is fracture spacing (cm), and  $b$  is the fracture aperture ( $\mu\text{m}$ ). The relation between fracture spacing, fracture aperture and fracture permeability is shown in Figure 5.

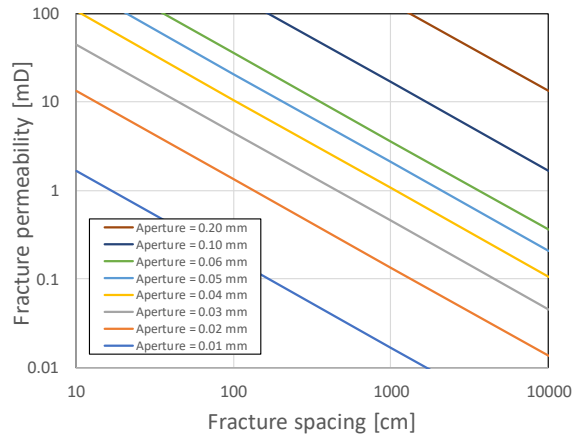


Figure 5. Relation between fracture spacing, fracture aperture and fracture permeability

#### 6.5. Karstification

Meteoric and hydrothermal karstification is one of the key parameters controlling the reservoir quality of the Dinantian carbonates in The Netherlands (Mozafari et al., 2019). Impact and extend of karstification events have been pinpointed in the cores obtained in the southern Dutch wells (e.g. KTG-01 and BHG-01) and speculated to be responsible for enhancement of reservoir quality in the CAL-GT wells. Nevertheless, the scarcity of samples

and lack of improved seismic images do not allow to quantitatively evaluate the karstification. For this reason, the presence of karsts has not been taken into account in the reservoir models. If, however, karsts are encountered in one of the wells, it will have a positive effect on the total geothermal power. The results presented in this report can therefore be seen as conservative in this perspective.

## 6.6. Benchmarking

A double porosity and a double permeability model were set up in Eclipse and compared against each other and against a semi-analytical model in Prosper. Input data for these three models are equal. Goal of this benchmarking exercise was to gain confidence in both approaches. The results of these three models is shown in Figure 6, where a fracture spacing of 1 per meter and a fracture aperture of 0.05 mm was assumed for each model. The effect of matrix permeability on the NCI of various scenarios is plotted.

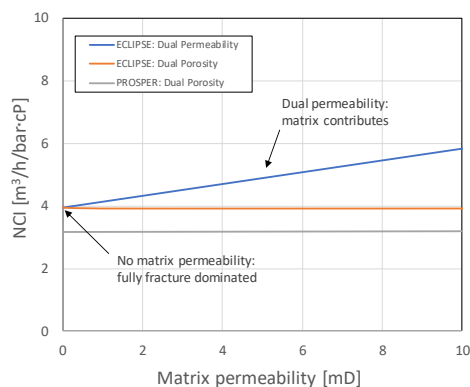


Figure 6. Benchmarking results of various mathematical approaches.

Figure 6 shows that for both dual porosity models, where matrix permeability is not accounted for, the results are comparable: assuming the same input data, but applying two completely different methodologies, results in NCIs that vary only by a factor 1.3. Moreover, applying the two numerical approaches (i.e. double porosity and double permeability), gives identical results if the assumption is made that the flow is fully fracture dominated. Increasing the matrix permeability results in increasing reservoir performance for the double permeability model, but not for the double porosity model. The observations thus made in Figure 6 give confidence that all approaches are correct. Since in real situations the matrix does contribute to flow, it is believed that dual permeability models are most representative; for this reason, only the double permeability model is used throughout the analysis in the subsequent chapters.

## 6.7. Input data and assumptions

Lithofacies including a range in reservoir properties (porosity and permeability) are described by Carlson (2019) and Mozafari et al. (2019) and are summarized in Table 1. The Dinantian geology in the Dutch subsurface has a large heterogeneity and the geological parameters vary a lot, as with all carbonate reservoirs. At the same time, there are many unknowns and large uncertainties for these parameters due to the shortage (or even absence) of data that could accurately describe the Dinantian reservoir characteristics to a more detailed level. Therefore, the decision was made to create several geological facies endmembers that are thought to

cover the range of possible scenarios. The matrix properties of these homogeneous reservoir models are shown in Table 1.

The lack of wells penetrating the Dutch Dinantian also results in large uncertainties regarding the typical fracture aperture and density for these carbonates; no discrete values for the fracture aperture and spacing can be given for a specific geographical region or geological facies endmember. Instead, a range in fracture aperture and spacing has been used, together with the four lithofacies endmembers described in Table 1, to calculate the NCI in Eclipse, using Eclipse's double permeability module. The full Eclipse deck is provided in the appendix. Note that for determination of the well's NCI, a single well only is needed in the deck.

*Table 1. Lithofacies classification deduced from Mozafari et al. (2019) and Carlson (2019). Porosity and permeability are average values based on the petrophysical evaluation by Carlson (2019).*

	Matrix porosity [%]	Matrix permeability [mD]
Dolomite	4	8
Platform	2	1
Basinal carbonate	0.5	0.1
Basinal shale	0	0

In the Eclipse deck the assumption is made that horizontal wells will be drilled, in order to increase the reservoir exposure to the wellbore and to increase the chance of hitting the most fracs, since fracs are expected to be mainly sub-vertical (> 60 deg) (Van Leverink and Geel, 2019). For modelling purposes, a horizontal wellbore of 1000 meter is assumed, with a wellbore diameter of 6 inch and a mechanical skin of 0 along the entire length of the well. The fracture permeability and fracture porosity are calculated using equations 8 and 9 and Table 1. Fracture aperture and fracture spacing do thus not form direct input into the Eclipse deck, but are incorporated into the fracture porosity and fracture permeability. Other important assumptions used in the double permeability model are given in Table 2. For various combinations of reservoir matrix properties (see Table 1) and fracture aperture and spacing, Eclipse calculates the well's Productivity Index based on the nine-point pressure average. This productivity index is subsequently multiplied with the reservoir's fluid viscosity at the prevailing temperature in order to obtain the NCI.

*Table 2. Main input parameters used for reservoir modelling.*

RESERVOIR MODELLING			
Top reservoir depth		4000	[m]
Reservoir dimensions (x, y, z)		6000 x 6000 x 500	[m]
Cell dimensions (x, y, z)		100 x 100 x 25	[m]
Number of matrix cells (x, y, z)		30 x 30 x 20	[-]
Number of fracture cells (x, y, z)		30 x 30 x 20	[-]
Number of fracture planes		3	[-]
NTG		1	[-]
kh/kv		1	[-]
Wellbore length		1000	[m]
Skin		0	[-]
Wellbore internal diameter		6	[inch]
Matrix porosity		variable, see table 1	[-]
Matrix permeability		variable, see table 1	[-]
Fracture spacing		variable	[-]
Fracture aperture		variable	[-]
Fracture porosity		variable, see equation 8	[-]
Fracture permeability		variable, see equation 9	[-]
Sigma		variable, see equation 4	[-]

## 6.8. Results

The results of the double permeability reservoir model, using the input data and assumptions described above, is graphically shown in Figure 7. For each of the lithofacies described in Table 1, the effect of fracture density and fracture aperture (lines) on the NCI is shown on the y-axis. Figure 7 also allows for the interpolation between various facies (e.g. a combination of two of the lithofacies), or the interpolation between fracture characteristics. Shown in this figure is that at large apertures the matrix permeability only has a very marginal effect.

A sensitivity analysis on this figure shows that if the fracture density is 1 (1/m) and the aperture is 0.05 (mm), then the NCI for the best reservoir lithofacies (dolomite) is 17 ( $\text{m}^3/\text{h}/\text{bar}\cdot\text{cP}$ ) and the NCI for the worst reservoir lithofacies (basinal shale) is 7.9 ( $\text{m}^3/\text{h}/\text{bar}\cdot\text{cP}$ ). In other words, the effect between the worst possible and the best possible matrix properties is a factor 2. A sensitivity analysis on the fracture properties however, shows that a small change in aperture from 0.04 mm to 0.05 mm can double the NCI. Also, a change in fracture density from 1 to 2 /m also results in a duplication of the NCI. In other words, a (very) small change in fracture properties (well within the uncertainty bandwidth described by Van Leverink and Geel, 2019) also results in a factor 2 difference in NCI. This shows that the fracture properties, which is the geological input carrying the most uncertainty, has by far the highest impact on the doublet performance.

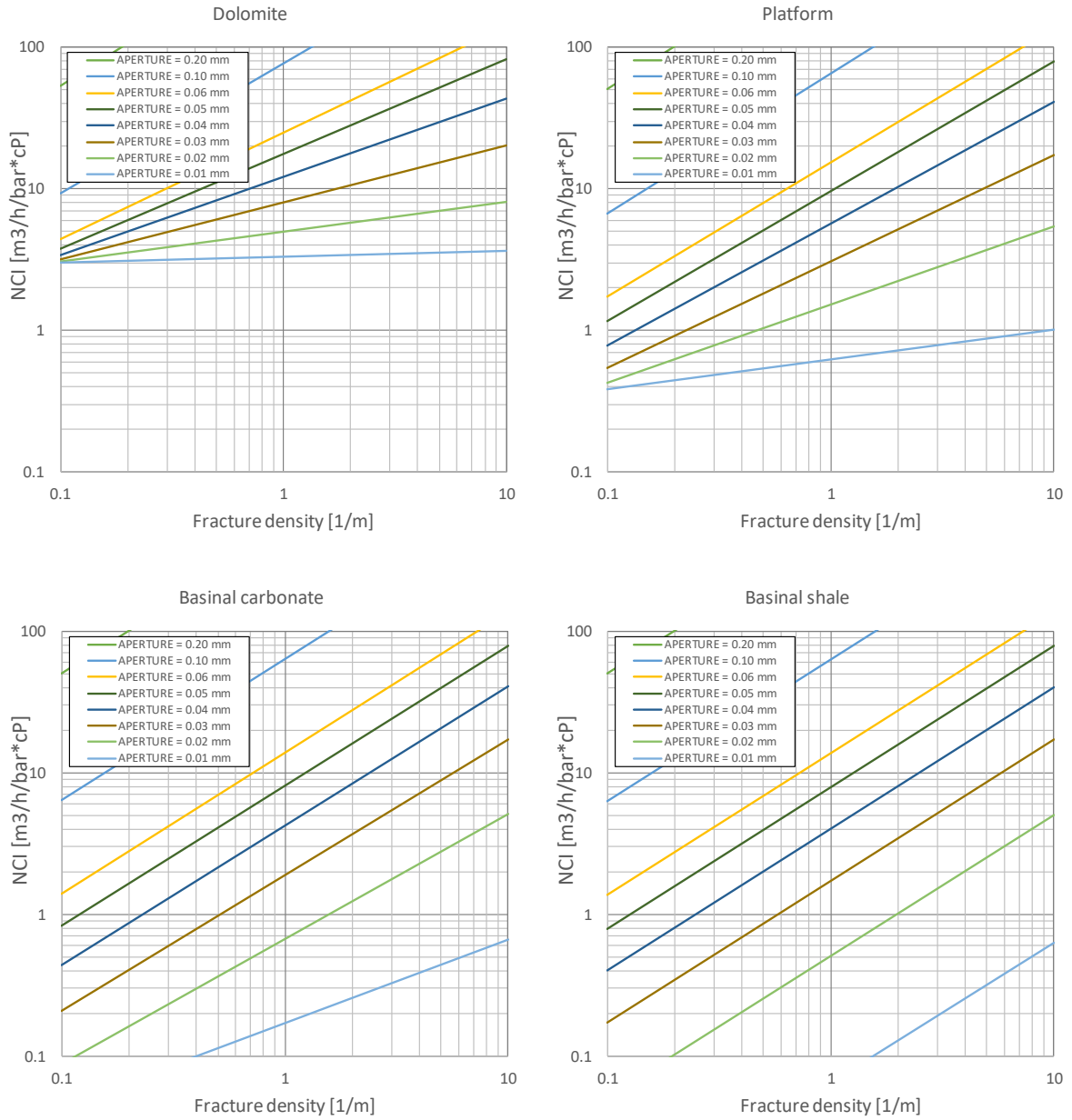


Figure 7. Results (NCI) of reservoir modelling of the four lithofacies in combination with various values for fracture density and fracture aperture.

## 7. Step 2: wellbore modelling

### 7.1. Doublet modelling

EBN's inhouse doublet simulator 'THOR' is used to calculate and amalgamate all pressure losses in a doublet system. THOR's core is formed by a set of fluid flow equations, relating pressure drop to flowrate. The various components or sections of the wells and their associated pressure drops or gains are shown in Figure 8. The sections used to determine the doublet's performance in this study are:

- $\Delta P_1$ : pressure losses in the reservoir (production side)
- $\Delta P_2$ : pressure losses across the production sandface and production completion
- $\Delta P_3$ : pressure losses along the production wellbore
- $\Delta P_4$ : pressure losses along the production casing
- $\Delta P_5$ : pressure gains inside the Electrical Submersible Pump (ESP)
- $\Delta P_6$ : pressure losses along the production tubing
- $\Delta P_7$ : pressure losses along the surface facilities
- $\Delta P_8$ : pressure losses and gains along the injection tubing
- $\Delta P_9$ : pressure losses and gains along the injection casing
- $\Delta P_{10}$ : pressure losses along the injection wellbore
- $\Delta P_{11}$ : pressure losses across the injection completion and injection sandface
- $\Delta P_{12}$ : pressure losses in the reservoir (injection side)

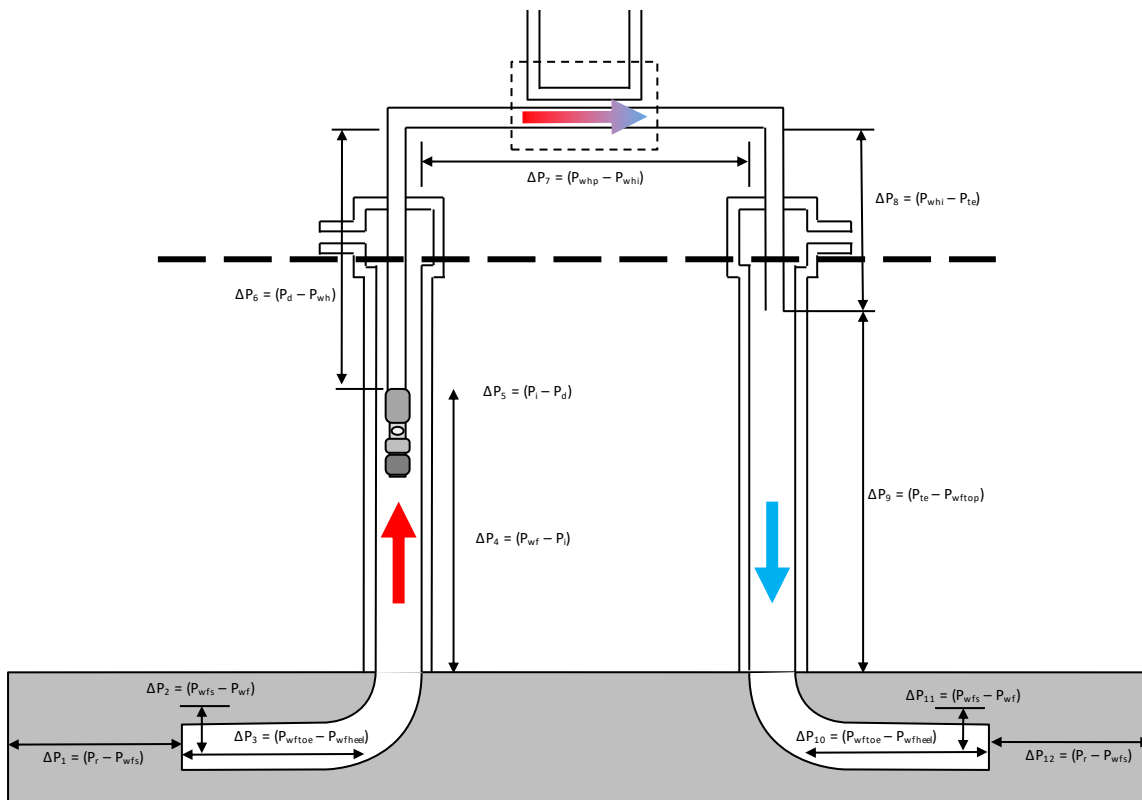


Figure 8. Schematic doublet model

The pressure losses inside the reservoir ( $\Delta P_1$  &  $\Delta P_{12}$ ) are calculated using Eclipse's double permeability model, which are converted into NCIs (see chapter 6). These NCIs serve as input in THOR and are thus representing the total pressure losses in the reservoir. The pressure losses across the sandface / completion ( $\Delta P_2$  &  $\Delta P_{11}$ ) and along the surface facilities are for the sake of simplicity assumed to be constant. The pressure losses along each of the

wellbores and pipes ( $\Delta P_3, \Delta P_4, \Delta P_6, \Delta P_8, \Delta P_9, \Delta P_{10}$ ) are calculated using the following equation, which includes viscous and gravitational effects:

$$\frac{dP}{dl} = - \frac{f\rho v^2}{2D} - g\rho \frac{dz}{dl} \quad [10]$$

where  $P$  is pressure (Pa),  $l$  is pipe section length (m),  $f$  is the Fanning friction factor as described by Beggs and Brill (1985),  $\rho$  is fluid density ( $\text{kg/m}^3$ ),  $v$  is in-situ fluid velocity (m/s),  $D$  is pipe inner diameter (m),  $g$  is the gravitational acceleration constant ( $9.80665 \text{ m/s}^2$ ), and  $z$  is the height (true vertical, m) of the pipe section. After simultaneously solving the pressure drop equations, the geothermal power is subsequently calculated using the following formula:

$$P_{gt} = Q_m c_p \Delta T_{he} \quad [11]$$

where  $P_{gt}$  is the geothermal power (W),  $Q_m$  is the mass flowrate (kg/s),  $c_p$  is the water's heat capacity ( $\text{J}/(\text{kgK})$ ) and  $\Delta T_{he}$  is the temperature difference between the inlet and the outlet of the heat exchanger ( $^{\circ}\text{K}$ ).

The pressure difference (head) to be generated by the ESP ( $\Delta P_5$ ) does not form one of the input variables for THOR; this pressure increase is calculated using a semi-analytical algorithm based on imposed injection pressure. As such, the ESP's pressure increase forms part of THOR's output.

SodM (2013) has issued a protocol with a guideline for the maximum allowable injection pressures. According to this document, the maximum bottomhole pressure is given by:

$$P_{wfi} = z \cdot g_1 \quad [12]$$

where  $P_{wfi}$  is the maximum acceptable flowing bottomhole pressure (bar) in the injector at the top reservoir level,  $z$  is the depth (m) in the injector at the top reservoir level, and  $g_1$  is a gradient based on the expected lowest minimal horizontal stress in the overlying formations, taking thermal effects into account. Exceeding this maximum allowable bottomhole pressure might result in fracture propagation at that level. From an operational point of view, it is more practical to adhere to a maximum allowable wellhead pressure, since downhole pressures are not always measured continuously. The maximum wellhead pressure is also given by SodM in the same document:

$$P_{whi} = z (g_1 - g_2) \quad [13]$$

where  $P_{whi}$  is the maximum allowable wellhead pressure (bar) at the injector,  $z$  is the depth to the top of the reservoir (m) and  $g_2$  is the hydraulic gradient of the injected water, which is a function of the salinity. In this conversion from bottomhole to wellhead conditions the frictional pressure losses are not taken into account.

The set-up of THOR is such that the geothermal power is calculated based on the maximum allowable surface injection pressures (equation 13). In these very deep and long UDG wells the friction inside the injection well can however be significant. Calculations based on the maximum tubinghead pressure are therefore an underestimation of the geothermal power; higher wellhead pressures are allowed as long as the maximum bottomhole pressures are not exceeded (equation 12). Despite being a (theoretical) underestimation, the decision was made to adhere to injection at maximum wellhead pressure. The main reason for this is that – especially in the case of narrow injection tubings – operating at maximum bottomhole

pressure results in unrealistically high wellhead pressures of several hundreds of bars. This is not only undesired from a safety point of view, technically this might not be possible at all.

The static temperature profile along the wells is calculated using equation 14:

$$T_z = T_{surface} + \lambda z \quad [14]$$

where  $T_z$  is the static temperature ( $^{\circ}\text{C}$ ) at a given depth,  $T_{surface}$  is the yearly average temperature at surface level ( $^{\circ}\text{C}$ ),  $\lambda$  is the geothermal gradient in The Netherlands ( $^{\circ}\text{C}/\text{m}$ ), and  $z$  is the depth (m) along the well. The heat loss or gains in both the production and injection well are calculated using the method proposed by Garcia-Gutierrez et al. (2001) and Mijnlief et al. (2014):

$$q_{w,well} = \frac{4\pi k_{t,g}(T_c - T_z)}{\ln\left(\frac{4\alpha_{t,g}t}{\sigma r_c^2}\right)} \quad [15]$$

$$\frac{dT_{well}}{dl} = \frac{q_{w,well}}{Q_m \cdot c_p} \quad [16]$$

where  $q_{w,well}$  is the heat loss per unit well length (W/m),  $k_{t,g}$  is the thermal conductivity of the rocks surrounding the well (W/(m·K)),  $T_c$  is the casing temperature ( $^{\circ}\text{K}$ ), considered to be equal to the temperature of the water in the well,  $T_z$  is the static temperature ( $^{\circ}\text{K}$ ) at a given depth,  $\alpha_{t,g}$  is the thermal diffusion coefficient of the aquifer rock ( $\text{m}^2/\text{s}$ ),  $t$  is the time since the start of heat flow, assumed to be 1 year,  $\sigma$  is  $e^{\gamma}$  ( $\gamma$  being Euler's constant) and  $r_c$  is the inner radius of the casing (m).  $T_{well}$  is the water temperature of the water in the well ( $^{\circ}\text{K}$ ),  $l$  is the length along the well (m),  $Q_m$  is the mass flowrate (kg/s) and  $c_p$  is the heat capacity of the water (J/(kgK)). Equations 14 to 16 are used to calculate the steady state production temperature.

The density of the water as a function of pressure, salinity and temperature is given by Batzle and Wang (1992):

$$\rho_{fw} = 1 + 10^{-6}(-80T - 3.3T^2 + 0.00175T^3 + 489P - 2TP + 0.016T^2P - 1.3 \cdot 10^{-5}T^3P - 0.333P^2 - 0.002TP^2) \quad [16]$$

$$\rho = \rho_{fw} + s(0.668 + 0.44s + 10^{-6}(300P - 2400Ps + T(80 + 3T - 3300s - 13P + 47PS))) \quad [17]$$

where  $\rho_{fw}$  is the fresh water density ( $\text{kg}/\text{m}^3$ ),  $\rho$  is the salt water density ( $\text{kg}/\text{m}^3$ ),  $P$  is the pressure (MPa),  $s$  is the salinity (ppm) and  $T$  is the temperature ( $^{\circ}\text{C}$ )

The water viscosity is calculated using the correlation given by Batzle and Wang (1992):

$$\mu = 0.1 + 0.333s + (1.65 + 91.9s^3)\exp(-(0.42(s^{0.8} - 0.17)^2 + 0.045)T^{0.8}) \quad [18]$$

where  $\mu$  is the water viscosity (cP),  $s$  is the salinity (ppm) and  $T$  is the temperature ( $^{\circ}\text{C}$ ).

The heat capacity is calculated using the Grunberg (1970) correlations:

$$C_p = (+5.328 - 9.760 \cdot 10^{-2}s + 4.040 \cdot 10^{-4}s^2) + (-6.913 \cdot 10^{-3} + 7.351 \cdot 10^{-4}s - 3.150 \cdot 10^{-6}s^2)T$$

$$\begin{aligned}
& +(+9.6 \cdot 10^{-6} - 1.927 \cdot 10^{-6}s + 8.230 \cdot 10^{-9}s^2)T^2 \\
& +(+2.5 \cdot 10^{-9} + 1.666 \cdot 10^{-9}s - 7.125 \cdot 10^{-12}s^2)T^3 \quad [19]
\end{aligned}$$

where  $c_p$  is the water heat capacity (kJ/(kgK)),  $s$  is the salinity (g/kg), and  $T$  is temperature ( $^{\circ}\text{K}$ ).

## 7.2. Input data and assumptions

As for the reservoir modelling (step 1), the wellbore modelling module assumes that the 1000 m horizontal wellbore section has an internal diameter of 6 inch, the roughness of which is assumed to be 1.3 milli inch. The assumption is made that all fractures are perfectly homogeneously distributed within the reservoir.

Since the depths, targets, and functional requirements etc. are unknown at this exploration phase, a rather simple geometric well model was assumed:

- Injector and producer have an identical well trajectory and target depth
- The production casing and tubing have a constant size (diameter) along their entire length.
- Since a horizontal reservoir penetration is assumed, the wells cannot be drilled vertically; consequently, the measured depth of the wells will be larger than the true vertical depth. The trajectories of the modelled wells are shown in Figure 9.

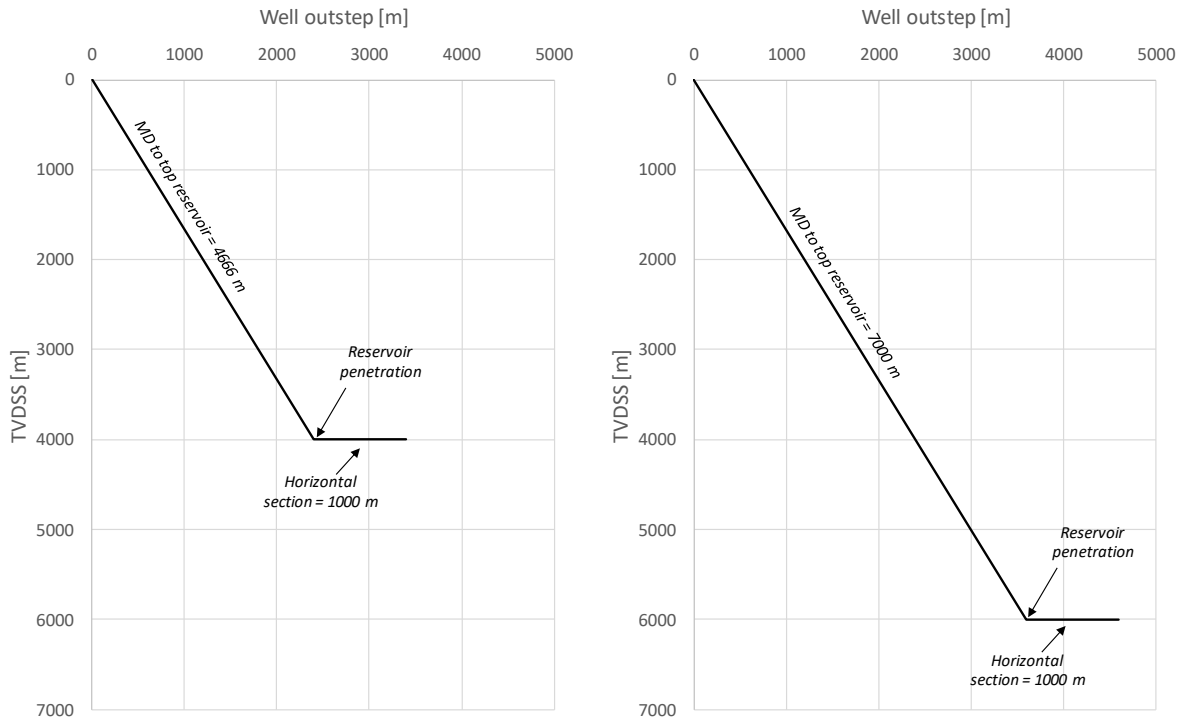


Figure 9. Well trajectory used throughout this study. For reservoirs located at a depth of 4000 m the well configuration is shown in the left picture. For reservoirs located at a depth of 6000 m the well configuration is shown in the right picture.

For Step 2 the assumption is made that the reservoir is normally (hydrostatically) pressured. As already discussed before, the model assumes that injection will be at the maximum allowable injection pressure. Other THOR modelling assumptions are described in Table 3.

Table 3. Main input parameters used for wellbore modelling.

WELLBORE MODELLING		
Wellbore length horizontal section	1000	[m]
Wellbore internal diameter	6	[inch]
Wellbore roughness	1.3	[milli-inch]
Pipe roughness	1.3	[milli-inch]
ESP efficiency	0.58	[-]
ESP setting depth	1000	[m TVDSS]
Pressure drop surface facilities	5	[bar]
Max allowable fluid gradient	0.135	[bar/m]
Geothermal gradient	0.031	[deg/m]
Distance producer - injector (heel to heel)	1500	[m]
Salinity	150000	[ppm]
Thermal conductivity of the overburden	3	[W/(m.K)]
Thermal diffusion coefficient aquifer rock	1.20E-06	[m <sup>2</sup> /s]
Yearly average surface temperature	10	[deg C]
Reservoir pressure	hydrostatic	[bar]
NCI	variable, from figure 7	[m <sup>3</sup> /h/bar·cP]
Tubing size	variable	[inch]
Reservoir depth	variable	[m]
Injection temperature	variable	[deg C]

### 7.3. Results

The wellbore modelling results, based the assumptions and input data described before, are shown in Figure 10. In this figure, the effect of tubing/casing internal diameter and NCI on the flowrate is shown. The better the reservoir performance, the higher the flowrate will be. Also, larger tubings/casings have less frictional pressure losses, resulting in higher flow rates as well.

Figure 10 shows the *mathematical* solution to the equations described in the previous chapters but does not take the operational aspects into account. One of these includes the maximum acceptable flowrates at any point within the entire system, such that the reservoir or hardware will not be damaged and that no erosion will take place. This maximum flow rate depends on many variables, including sand- and gas-content, hardware dimensions, metallurgy, etc. and is often related to the velocity of the water rather than the flux. Even if the reservoir and/or the wells can initially deliver these volumes, it is not recommended to exceed this threshold value. Without a detailed well design, it is not possible to determine what that maximum flow rate will be, although flow rates above a certain threshold value will undoubtedly cause permanent damage. A first pass approximation of this maximum operational flow rate is  $\sim 500 \text{ m}^3/\text{h}$ , although this varies widely from one well to the other.

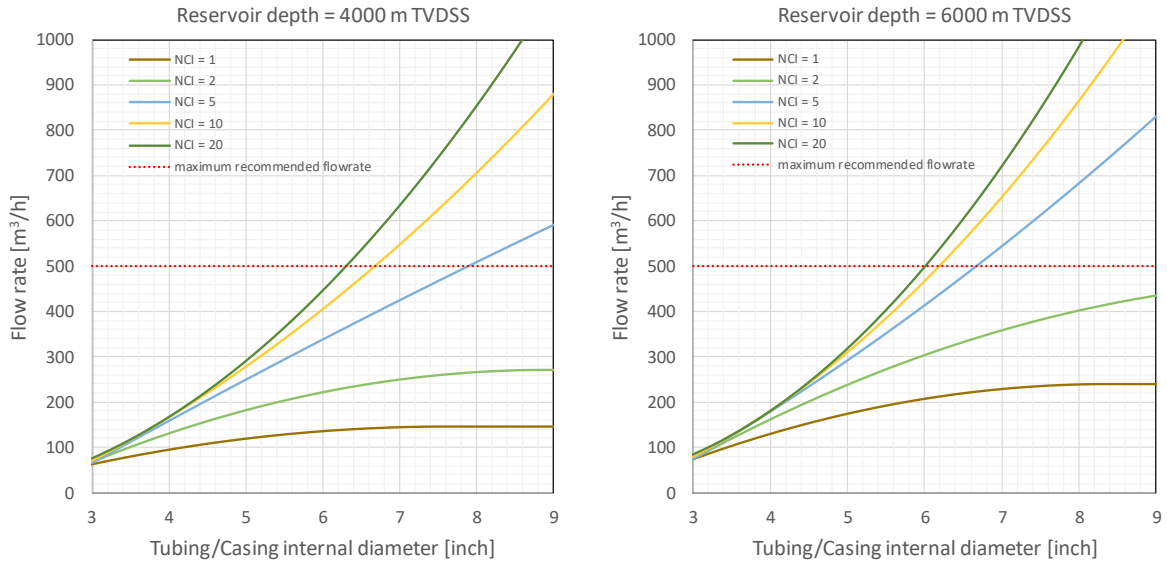


Figure 10. Wellbore modelling results (flow rate) for a reservoir at a depth of 4000 m (left) and a reservoir at a depth of 6000 m (right). Note that the deeper the reservoir, the higher the maximum injection pressure is (equations 12 and 13). Consequently, the flowrate for the deeper reservoir (right picture) is higher than the flowrate for shallow reservoirs (left picture), despite the additional friction losses inside the tubing/casing due to increased well length. Red dotted line is a rough approximation of the maximum recommended flowrate, although this varies widely from well to well.

The geothermal power is calculated using the flow rate, the water's heat capacity and the difference between the inlet and the outlet of the heat exchanger, see equation 11. These results are shown in Figure 11. Once the reservoir depth, the NCI and the injection temperature are known, and a decision is made on the desired internal diameter of the tubings and production casings, then the geothermal power of that doublet can be read off on the vertical axis. This figure allows for the interpolation of depths in between 4000 and 6000 meters, or of injection temperatures in between 35 and 55 °C.

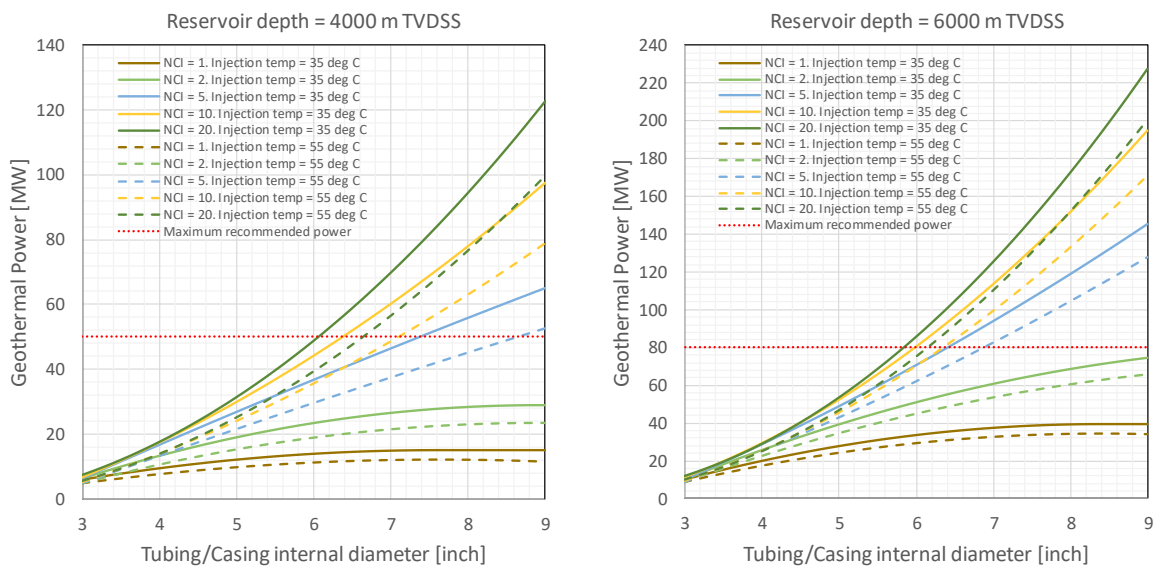


Figure 11. Wellbore modelling results (geothermal power) for a reservoir at a depth of 4000 m (left) and a reservoir at a depth of 6000 m (right). Solid lines indicate the geothermal power in case of an injection temperature of 35 °C, while the dashed lines indicate a geothermal power in case of an

*injection temperature of 55 °C. For both pictures the assumption is made that the reservoir is normally pressured (i.e. hydrostatic pressure). Red horizontal dotted line is a rough approximation of the maximum power that can be achieved, based on the maximum achievable flowrate, but this varies widely from well to well.*

An analysis of Figure 11 reveals that the geothermal power increases with improved reservoir performance (NCI) and with increasing tubing / casing size. Due to the higher reservoir temperatures at a depth of 6000 m the geothermal power significantly increases with depth as well. Figure 11 also shows that if the reservoir is of poor quality (e.g. NCI of 1) the effect of increasing the tubing/casing sizes only has a marginal impact. If, however, the reservoir is of good quality (e.g. NCI of 5 or larger, a too small tubing will significantly hinder the geothermal power. The recommendation would be to drill large wells, albeit that large wells have a big impact on the expenditures, most notably the CAPEX. The challenge will therefore be to drill large enough wells at low costs, in order to optimize the commercial and economical aspects of the business cases. Once an estimation of the total expenditures has been made, the required geothermal power needed to achieve a positive Net Present Value (NPV) can be calculated. It is recommended to perform such an economic analysis to assess the lower limit of geothermal power for an UDG doublet.

Care must also be taken not to exceed the well's maximum operational flowrate, which is in this document assumed to be ~ 500 m<sup>3</sup>/h. This value can be converted to a maximum recommended power. A good approximation for the maximum recommended geothermal power is ~ 50 MW for reservoirs at 4000 m and ~ 80 MW for reservoirs at 6000 m. This technical upper limit in combination with the economic lower limit, results in a certain bandwidth of geothermal power that doublets must have. If the performance falls outside this bandwidth, the project will not be economically viable: either the revenues will be too low, or the operational costs associated with remedial repair of the hardware will be too high. The challenge will therefore be to explore the Dutch Dinantian for good enough reservoir properties and drilling large enough wells, while simultaneously minimizing the expenditures and not exceeding the technical limits of the doublet.

## 8. Step 3: Compensation for overpressure

SodM (2013) states that the maximum allowable injection pressure at the top-reservoir level can be calculated using equation 13. This formula is based on the expected lowermost value of the fracture propagation pressure. The fracture propagation pressure is independent of the reservoir pressure; it does not change if the reservoir is overpressured. The difference between the flowing bottomhole pressure and the absolute reservoir pressure (“drawdown”) largely dictates the injectivity of the well; the higher this drawdown, the higher the flowrates and hence the geothermal power of the doublet will be. This implies that if reservoirs are overpressured, the allowable drawdown will be less, resulting in lower flowrates and consequently lower geothermal power.

Some of the wells drilled through the Dutch Dinantian have shown significant overpressure, or reservoir pressures that are higher than the hydrostatic pressure for brine saturated reservoirs: Uithuizermeeden (UHM-02) had an overpressure of ~140 bar overpressure, while Luttelgeest (LTG-01) had an overpressure of ~ 104 bar (Carlson, 2019). This overpressure will have a negative effect on the performance of the doublet. An additional step (Step 3) is added to the workflow, which can be used to determine the impact overpressure can or will have on the geothermal power.

### 8.1. Input data and assumptions

For the determination of the effect of overpressure on the geothermal power, the same assumptions are made as for the calculation of the geothermal power for hydrostatically pressured reservoir, see chapter 7. The only exception is the reservoir pressure, on which a sensitivity was done in this step.

### 8.2. Results

The effect of overpressure on the geothermal power is shown in Figure 12, from which the reduction in geothermal power per bar overpressure can be read off. If the absolute value of the overpressure is known (or assumed), then the total reduction in geothermal power can be deduced.

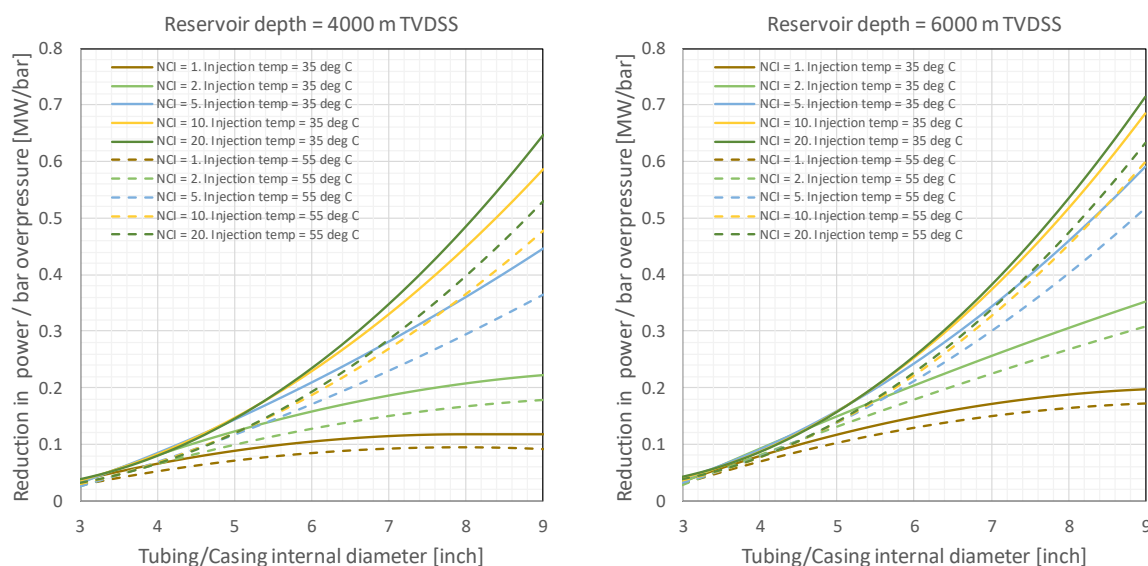


Figure 12. Effect of overpressure on the geothermal performance of doublets. Left picture: results for a reservoir at a depth of 4000 m; right picture: results for a reservoir at a depth of 6000 m. Solid lines indicate the reduction in geothermal power per bar overpressure in case of an injection

temperature of 35 °C, while the dashed lines indicate the reduction in geothermal power per bar overpressure in case of an injection temperature of 55 °C.

## 9. Workflow summary and example

The various steps described above to calculate the geothermal power are visualized schematically in Figure 13.

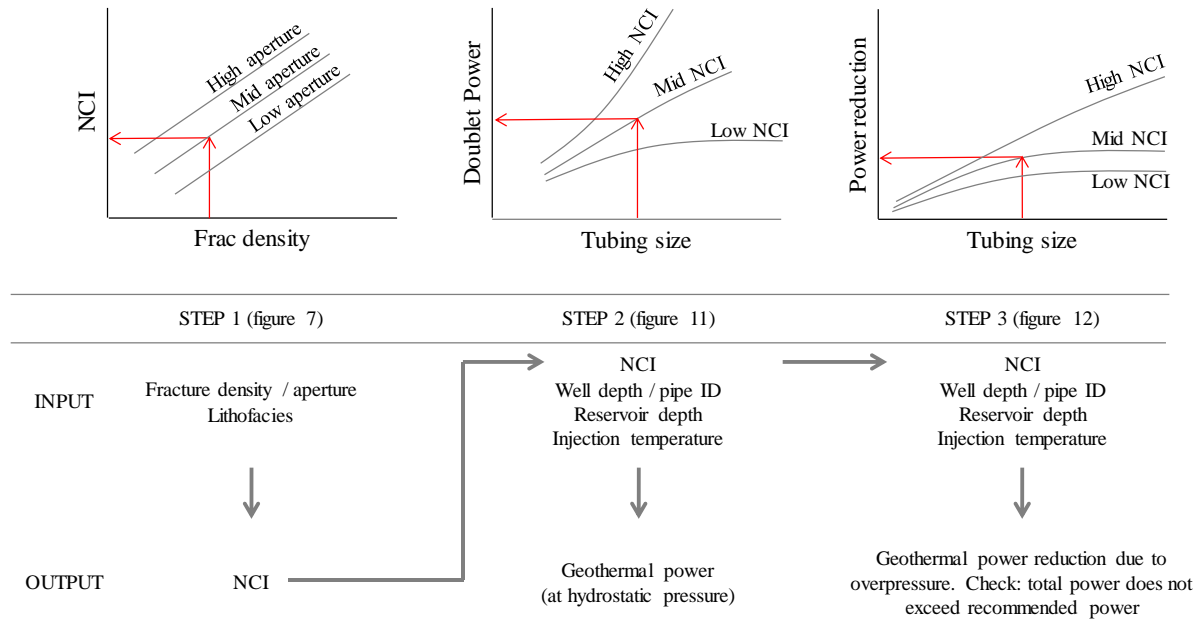


Figure 13. Workflow undertaken in this study.

### 9.1. Example

**Question:** Assume that the following geological input parameters are known: reservoir depth is 4000 m, overpressure is 100 bar, fracture density is 1 frac per meter, fracture aperture is 0.05 mm, the matrix consists of a platform, the tubing and casing sizes are 8 inch, and the injection temperature is 35 °C. What is the geothermal power for this doublet?

**Answer:** Step 1: based on the given lithofacies and the fracture characteristics, the NCI is 9.5 (m<sup>3</sup>/h/bar·cP), see Figure 7. Step 2: based on the NCI of 9.5 and the given tubing size and reservoir depth, the anticipated flow rate is 680 m<sup>3</sup>/h, see Figure 10. Based on an injection temperature of 35 °C, the geothermal power will therefore be 76 MW, see Figure 11. Care must be taken with the result, since 680 m<sup>3</sup>/h might very well be higher than the recommended operational maximum flowrate of ~ 500 m<sup>3</sup>/h. However, the reservoir is overpressured, which restricts the doublet in its performance. Step 3: Based on the NCI of 9.5 and the given tubing size, reservoir depth and injection temperature, the reduction in geothermal power is 0.44 MW/bar, see Figure 12. Based on the given overpressure of 100 bar, the total reduction in geothermal power is 0.44 MW/bar x 100 bar = 44 MW. The geothermal power for this doublet is therefore 76 MW – 44 MW = 32 MW. This value is below the recommended maximum geothermal power of 50 MW for reservoirs at 4000 m.

## 10. Conclusions

The method provided in this document allows the user to determine the geothermal power of fractured carbonate reservoirs, which fully depends on the chosen combination of input variables. Given the wide range in possible geological - and well scenario's, it is very hard to quantify the geothermal capacity of the Dinantian. Although many variables can be chosen with a certain degree of confidence, some unknown variables have a large impact on the possible outcomes. These can be subdivided into geological uncertainty and well uncertainty.

The geological uncertainty involves fracture aperture, fracture spacing, reservoir matrix properties (porosity and permeability), reservoir depth and reservoir pressure. The wide range in (the combination of) geological input parameters results unavoidably in a wide range in possible outcomes. With the currently available geological and geophysical data set, this range cannot be narrowed down any further.

Well uncertainty mainly involves the size of the wells. Big bore wells display a significant advantage over wells with a smaller diameter, especially if the reservoir deliverability is high. Large wells however come with higher costs, and as such the well size is a financial decision, rather than an uncertainty.

In case of very good reservoir properties, and adhering to the legal injection limits, a technical upper limit for the flowrates prevents unconstrained production and injection. In case of too poor reservoir properties however, the geothermal power might not be high enough to achieve a positive NPV. For future studies, this bandwidth in geothermal power must be explored further in order to assess the economic viability of UDG doublets.

## 11. References

- Batzle, M., & Wang, Z. (1992). Seismic properties of pore fluids. *Geophysics*, Vol. 57, 1396-1408.
- Beggs, H., & Brill, J. (1973). A study of two-phase flow in inclined pipes. *Journal of Petroleum Technology*, May 1973, 607-617.
- Bouroullec, R., Nelskamp, S., Kloppenburg, A., Abdul Fattah, R., Foeken, J.P.T., ten Veen, J.H., Geel, C.R., Debacker, T., Smit, J. (2019) Burial and Structural Analysis of the Dinantian Carbonates in the Dutch Subsurface (SCAN). Downloadable from [www.nlog.nl](http://www.nlog.nl)
- Boxem, T. A. P., Veldkamp, J. G., and van Wees, J. D. A. M. (2016). Ultra-diepe geothermie: Overzicht, inzicht & to-do ondergrond. TNO report, R10803, 53 pp.
- Carlson, T. (2019). Petrophysical Report of the Dinantian Carbonates in the Dutch Subsurface (SCAN). Downloadable from: [https://www.nlog.nl/sites/default/files/2019-08/scan\\_dinantien\\_petrophysics\\_report.pdf](https://www.nlog.nl/sites/default/files/2019-08/scan_dinantien_petrophysics_report.pdf)
- Dake, L.P. 1978. *Fundamentals of Reservoir Engineering*. Amsterdam, Elsevier Science BV.
- Garcia-Gutierrez, A., Espinosa-Paredes, G., & Hernandez-Ramirez, I. (2001). Study on the flow production characteristics of deep geothermal wells. *Geothermics*, Vol. 31, 141-167.
- Grunberg, L. (1970). Properties of sea water concentrations. *Third International Symposium on Fresh Water from the Sea*, Vol. 1, pp. 31-39.
- Kazemi, H., Merrill JR., L. S., Porterfield, K. L., and Zeman, P. R. "Numerical Simulation of Water-Oil Flow in Naturally Fractured Reservoirs," paper SPE 5719, *Society of Petroleum Engineers Journal* (1976) 16, No. 6, 317-326.
- Mijnlieff, H.F., Obdam, A.N.M., Van Wees, J.D.A.M., Pluymaekers, M.P.D., and Veldkamp, J.G. (2014). DoubletCalc 1.4 manual English version for DoubletCalc 1.4.3. TNO report 2014 R11396
- Mozafari, M., Gutteridge, P., Riva, A., Geel, C. R., Garland, J., and Dewit, J. (2019). Facies analysis and diagenetic evolution of the Dinantian carbonates in the Dutch subsurface (SCAN). Downloadable from [www.nlog.nl](http://www.nlog.nl)
- Petroleum Experts (2019). PROSPER Multiphase Well and Pipeline Nodal Analysis. <http://www.petex.com/products/ipm-suite/prosper/>
- Reiss, L. H. (1980). *The Reservoir Engineering Aspects of Fractured Formations*. Editions TECHNIP.
- Schlumberger (2019). Eclipse Reservoir Engineering Software. [www.software.slb.com](http://www.software.slb.com)
- SodM, TNO-AGE (23 november 2013). Protocol bepaling maximale injectiedrukken bij aardwarmtewinning. <https://www.sodm.nl/documenten/publicaties/2013/11/23/protocol-bepaling-maximale-injectiedrukken-bij-aardwarmtewinning>
- Van Leverink, D.J. and Geel, C.R. (2019). Fracture Characterization of the Dinantian Carbonates in the Dutch Subsurface (SCAN). Downloadable from: [www.nlog.nl/scan](http://www.nlog.nl/scan)
- Warren, J. E., & Root, P. J. (1963). *The Behavior of Naturally Fractured Reservoirs*. Society of Petroleum Engineers. SPE-426-PA

## 12. Appendix: Eclipse deck

```
RUNSPEC
TITLE

DIMENS
 60 60 40 /

DUALPORO

DUALPERM

WATER

GAS

METRIC

EQLDIMS
 1 500 2 1 1 /

TABDIMS
 2 1 13 13 2 5 /

REGDIMS
 2 1 0 0 /

WELLDIMS
 2 100 1 4 /

NUPCOL
 4 /

START
 01 'JAN' 2024 /

NSTACK
 4 /

UNIFOUT

GRID =====

NODPPM

EQUALS
'DX' 100 / MATRIX AND FRACTURES
'DY' 100 /
'DZ' 25 /
'PORO' 0.04 1 60 1 60 1 20 / MATRIX
'PERMX' 8 1 60 1 60 1 20 /
'PERMY' 8 1 60 1 60 1 20 /
'PERMZ' 8 1 60 1 60 1 20 /
'PORO' 0.006 1 60 1 60 21 40 / FRACTURES
'PERMX' 13392 1 60 1 60 21 40 /
'PERMY' 13392 1 60 1 60 21 40 /
'PERMZ' 13392 1 60 1 60 21 40 /
'TOPS' 4000 1 60 1 60 1 1 /
/

RPTGRID
'DX'
'DY'
'DZ'
'PERMX'
'PERMY'
'MULTX'
'MULTY'
```

'PORO'  
'TOPS'  
'PORV'  
'DEPTH'  
'TRANX'  
'TRANY'  
'ALLNNC'  
/

SIGMA  
1200 /

DEBUG  
6\*0 1 0 /

INIT

PROPS =====

SWFN

0.0 0.0 0  
0.1 0.1 0  
0.2 0.2 0  
0.3 0.3 0  
0.4 0.4 0  
0.5 0.5 0  
0.6 0.6 0  
0.7 0.7 0  
0.8 0.8 0  
0.9 0.9 0  
1.0 1.0 0

/

0.0 0.0 0  
0.1 0.1 0  
0.2 0.2 0  
0.3 0.3 0  
0.4 0.4 0  
0.5 0.5 0  
0.6 0.6 0  
0.7 0.7 0  
0.8 0.8 0  
0.9 0.9 0  
1.0 1.0 0

/

SGFN

0.0 0.0 0.0  
0.7 1.0 0.0

/

0.0 0.0 0.0  
0.7 1.0 0.0

/

PVTW

400 1.0 0.0000032 0.19358 0.00E-01 /

PVDG

14.7 27.71 0.0138  
5014.0 0.69457 0.0262

/

DENSITY

850 1029.77 1 /

RPTPROPS

'PRES' 'SOIL' 'SWAT' 'RS' 'FIP=2' 'EQUIL' /

ROCK

400 1.00E-05 /  
400 5.00E-03 /

REGIONS =====

RPTREGS  
'SATNUM'  
/

SOLUTION =====

SWAT  
144000\*1.0 /

PRVD  
4000 400  
4200 420 /

RPTSOL  
'PRES' 'SWAT' 'RS' 'FIP=2' 'EQUIL' /

SUMMARY =====

TCPU  
PERFORMA  
ALL  
SEPARATE  
WPI9  
/

SCHEDULE =====

TSTEP  
1.0 /

RPTSCHED  
'PRES' 'SWAT' 'RESTART=2' 'FIP=2' 'WELLS=2' 'SUMMARY=2' 'NEWTON=2' /

WELSPECS  
'PROD1' 'P' 35 30 4000 'WATER'  
/

COMPDAT  
'PROD1' 35 30 10 10 'OPEN' 0 1\* 0.2159 1\* 0 0 X/  
'PROD1' 34 30 10 10 'OPEN' 0 1\* 0.2159 1\* 0 0 X/  
'PROD1' 33 30 10 10 'OPEN' 0 1\* 0.2159 1\* 0 0 X/  
'PROD1' 32 30 10 10 'OPEN' 0 1\* 0.2159 1\* 0 0 X/  
'PROD1' 31 30 10 10 'OPEN' 0 1\* 0.2159 1\* 0 0 X/  
'PROD1' 30 30 10 10 'OPEN' 0 1\* 0.2159 1\* 0 0 X/  
'PROD1' 29 30 10 10 'OPEN' 0 1\* 0.2159 1\* 0 0 X/  
'PROD1' 28 30 10 10 'OPEN' 0 1\* 0.2159 1\* 0 0 X/  
'PROD1' 27 30 10 10 'OPEN' 0 1\* 0.2159 1\* 0 0 X/  
'PROD1' 26 30 10 10 'OPEN' 0 1\* 0.2159 1\* 0 0 X/  
'PROD1' 25 30 10 10 'OPEN' 0 1\* 0.2159 1\* 0 0 X/  
'PROD1' 35 30 30 30 'OPEN' 0 1\* 0.2159 1\* 0 0 X/  
'PROD1' 34 30 30 30 'OPEN' 0 1\* 0.2159 1\* 0 0 X/  
'PROD1' 33 30 30 30 'OPEN' 0 1\* 0.2159 1\* 0 0 X/  
'PROD1' 32 30 30 30 'OPEN' 0 1\* 0.2159 1\* 0 0 X/  
'PROD1' 31 30 30 30 'OPEN' 0 1\* 0.2159 1\* 0 0 X/  
'PROD1' 30 30 30 30 'OPEN' 0 1\* 0.2159 1\* 0 0 X/  
'PROD1' 29 30 30 30 'OPEN' 0 1\* 0.2159 1\* 0 0 X/  
'PROD1' 28 30 30 30 'OPEN' 0 1\* 0.2159 1\* 0 0 X/  
'PROD1' 27 30 30 30 'OPEN' 0 1\* 0.2159 1\* 0 0 X/  
'PROD1' 26 30 30 30 'OPEN' 0 1\* 0.2159 1\* 0 0 X/  
'PROD1' 25 30 30 30 'OPEN' 0 1\* 0.2159 1\* 0 0 X/  
/

WCONPROD  
'PROD1','OPEN','WRAT' 0 1000 0 /  
/

```
TSTEP  
10*1  
/  
END
```

*This page intentionally left blank*

# Onderzoek in de ondergrond voor aardwarmte